ОБЪЕДИНЕННЫЙ
ИНСТИТУТ
ЯДЕРНЫХ
ИССЛЕДОВАНИЙ

Дубна

E17-2006-96

N. M. Plakida[1,2], V. S. Oudovenko[1,3]

ELECTRONIC SPECTRUM OF HIGH-TEMPERATURE CUPRATE SUPERCONDUCTORS

Submitted to «ЖЭТФ»

[1] Joint Institute for Nuclear Research, Dubna, Russia
[2] Max-Planck-Institut für Physik komplexer Systeme, Dresden, Germany
[3] Rutgers University, New Jersey, USA

2006

1. INTRODUCTION

Recent high-resolution angle-resolved photoemission spectroscopy (ARPES) studies revealed a complicated character of electronic structure and quasiparticle (QP) spectra in copper-oxide superconductors. In particular, a pseudogap in the electronic spectrum and an arc-type Fermi surface at low doping were revealed, a substantial wave-vector and energy-dependent renormalization of the QP dispersion («kinks») was observed (for a review, see [1,2]). As was originally pointed out by Anderson [3], strong electron correlations in cuprates play an essential role in explaining their normal and superconducting properties.

A conventional approach in describing strong electron correlations is based on consideration of the Hubbard model. It has some advantages in comparison with the $t-J$ model which can be derived from the Hubbard model in the limit of strong correlations. Namely, the Hubbard model allows to study a moderate correlation limit observed experimentally in cuprates and more consistently takes into account a two-subband character of electronic structure, in particular, a weight transfer between subbands with doping. Various methods were proposed to study electronic structure within the Hubbard model. An unbiased method is based on numerical simulations for finite clusters (for a review see, e. g., [4]) which, however, precludes to study subtle features of QP spectra due to poor energy and wave-vector resolutions in small size clusters. In analytical calculations of spectra mean-field type approximations are often used (for a review, see [5]) which cannot reproduce the above-mentioned effects caused by the self-energy contributions. In the dynamical mean-field theory (DMFT) (for a review, see [6, 7]) the self-energy is treated in the single-site approximation which also unable to describe wave-vector-dependent phenomena. To overcome this flaw of DMFT, various types of the dynamical cluster theory were developed (for a review, see [8, 9]). In these methods a restricted wave vector and energy resolutions can be achieved depending on the size of the cluster. By including into the DMFT scheme an additional momentum-dependent self-energy originating from short-range antiferromagnetic (or charge) correlations, a pseudogap state in the Hubbard model was obtained [10]. At the same time, an equation of motion method for the thermodynamic Green functions (GF) [11] appears to be successful in describing physical properties of the Hubbard model (for a review, see [12]). By taking into account the self-energy corrections in this method, one can try to explain the peculiarity of the ARPES spectra in cuprates. For instance, calculation

of electronic spectrum within the first order perturbation theory for the self-energy has reproduced quite accurately quantum Monte Carlo results [13], while application of an incremental cluster expansion for the self-energy has enabled to observe the kink structure in the QP spectrum [14].

In the present paper, we study an effective Hubbard model reduced from the p–d model for the CuO_2 plane in cuprates. We apply the Mori-type projection technique in the equation of motion method for the thermodynamic GF in terms of the Hubbard operators elaborated in our previous publications [15–17]. A self-consistent solution of the Dyson equation for the model with a self-energy derived in the noncrossing approximation (NCA) beyond a perturbation approach is reported. A dispersion of single-particle excitations, the Fermi surface and spectral functions are calculated. In particular, we study a hole-doped case. At low hole concentrations the Fermi surface (FS) reveals an arc-type shape with pseudogaps in the $(\pi, 0)$ region of the Brillouin zone (BZ). A strong renormalization effects of the dispersion close to the Fermi energy («kinks») are observed due to electron scattering on antiferromagnetic (AF) spin fluctuations induced by kinematic interaction for the Hubbard operators. Electron occupation numbers show only a small drop at the Fermi energy. For high temperature or large hole concentrations AF correlations become irrelevant and a crossover to a Fermi liquid-like behavior is observed.

In the next section we briefly discuss the model and derivation of the Dyson equation and the self-energy calculation in the NCA. The results of numerical solution of the self-consistent system of equations for various hole concentrations in the model are presented in Sec. 3. Conclusions are given in Sec. 4.

2. GENERAL FORMULATION

2.1. Effective Hubbard Model and Dyson Equation. Following a cell-cluster perturbation theory (e. g., [15,18,19]) based on a consideration of the original two-band p–d model for the CuO_2 layer [20] we consider an effective two-dimensional Hubbard model for holes

$$\begin{aligned} H &= \varepsilon_1 \sum_{i,\sigma} X_i^{\sigma\sigma} + \varepsilon_2 \sum_i X_i^{22} + \sum_{i \neq j,\sigma} \{ t_{ij}^{11} X_i^{\sigma 0} X_j^{0\sigma} \\ &+ t_{ij}^{22} X_i^{2\sigma} X_j^{\sigma 2} + 2\sigma t_{ij}^{12} (X_i^{2\bar{\sigma}} X_j^{0\sigma} + \text{H.c.}) \}, \end{aligned} \tag{1}$$

where $X_i^{nm} = |in\rangle\langle im|$ are the Hubbard operators (HOs) for the four states $n, m = |0\rangle, |\sigma\rangle, |2\rangle = |\uparrow\downarrow\rangle$, $\sigma = \pm 1/2 = (\uparrow, \downarrow)$, $\bar{\sigma} = -\sigma$. Here $\varepsilon_1 = \varepsilon_d - \mu$ and $\varepsilon_2 = 2\varepsilon_1 + U_{\text{eff}}$, where μ is the chemical potential. The effective Coulomb energy in the Hubbard model (1) is the charge-transfer energy $U_{\text{eff}} = \Delta = \epsilon_p - \epsilon_d$. The superscripts 2 and 1 refer to the two-hole p–d singlet subband and the one-hole

subband, respectively. According to the cell-cluster perturbation theory, we can take similar values for the hopping parameters in (1): $t_{ij}^{22} = t_{ij}^{11} = t_{ij}^{12} = t_{ij}$. The bare electron dispersion defined by the hopping parameter t_{ij} we determine by the conventional equation

$$t(\mathbf{k}) = 4t\,\gamma(\mathbf{k}) + 4t'\,\gamma'(\mathbf{k}) + 4t''\,\gamma''(\mathbf{k}), \tag{2}$$

where t, t', t'' are the hopping parameters for the nearest neighbor (n.n.) $(\pm a_x, \pm a_y)$, the next nearest neighbor (n.n.n.) $\pm(a_x \pm a_y)$ and $\pm 2a_x, \pm 2a_y$ sites, respectively, and $\gamma(\mathbf{k}) = (1/2)(\cos k_x + \cos k_y)$, $\gamma'(\mathbf{k}) = \cos k_x \cos k_y$ and $\gamma''(\mathbf{k}) = (1/2)(\cos 2k_x + \cos 2k_y)$ (the lattice constants $a_x = a_y$ equal to unity). To get a physically reasonable value for the charge-transfer gap for the conventional value of $t \simeq 0.4$ eV we take $\Delta = U_{\text{eff}} = 8t \simeq 3.2$ eV. The bare bandwidth is $W = 8t \simeq U_{\text{eff}}$ which shows that the effective p–d Hubbard model (1) corresponds to the strong correlation limit. In what follows, we take as an energy unit $t = 1$ and put $\varepsilon_d = 0$ in ε_1. The chemical potential μ depends on the average *hole* occupation number

$$n = 1 + \delta = \langle \sum_\sigma X_i^{\sigma\sigma} + 2X_i^{22} \rangle. \tag{3}$$

The HOs entering (1) obey the completeness relation $X_i^{00} + X_i^{\uparrow\uparrow} + X_i^{\downarrow\downarrow} + X_i^{22} = 1$ which rigorously preserves the constraint of no double occupancy of any quantum state $|in\rangle$ at each lattice site i. Due to the projected character of the HOs, they have complicated commutation relations $\left[X_i^{\alpha\beta}, X_j^{\gamma\delta}\right]_\pm = \delta_{ij}\left(\delta_{\beta\gamma} X_i^{\alpha\delta} \pm \delta_{\delta\alpha} X_i^{\gamma\beta}\right)$, which results in the so-called *kinematic interaction*. The upper sign here refers for the Fermi-like HOs like $X_i^{0\sigma}$ and the lower sign is for the Bose-like ones, like the spin or number operators.

To discuss the electronic structure within the model (1), we introduce a thermodynamic matrix Green function (GF) [11]

$$\hat{G}_{ij\sigma}(t - t') = \langle\langle \hat{X}_{i\sigma}(t) \,|\, \hat{X}_{j\sigma}^\dagger(t') \rangle\rangle = -i\theta(t - t')\langle\{\hat{X}_{i\sigma}(t),\, \hat{X}_{j\sigma}^\dagger(t')\}\rangle \tag{4}$$

in terms of the two-component operators $\hat{X}_{i\sigma} = \begin{pmatrix} X_i^{\sigma 2} \\ X_i^{0\bar{\sigma}} \end{pmatrix}$ and $\hat{X}_{i\sigma}^\dagger = (X_i^{2\sigma}\; X_i^{\bar{\sigma}0})$. To calculate the GF (4), we apply the Mori-type projection technique by writing equations of motion for the Heisenberg operators in the form:

$$\hat{Z}_{i\sigma} = [\hat{X}_{i\sigma},\, H] = \sum_j \hat{\varepsilon}_{ij\sigma} \hat{X}_{j\sigma} + \hat{Z}_{i\sigma}^{(\text{ir})}, \tag{5}$$

where the *irreducible* $\hat{Z}$-operator is determined by the orthogonality condition:

$$\langle\{\hat{Z}_{i\sigma}^{(\text{ir})},\, \hat{X}_{j\sigma}^\dagger\}\rangle = \langle \hat{Z}_{i\sigma}^{(\text{ir})}\, \hat{X}_{j\sigma}^\dagger + \hat{X}_{j\sigma}^\dagger\, \hat{Z}_{i\sigma}^{(\text{ir})} \rangle = 0. \tag{6}$$

This defines the frequency matrix

$$\hat{\varepsilon}_{ij} = (\{[\hat{X}_{i\sigma}, H], \hat{X}^{\dagger}_{j\sigma}\})\, \hat{Q}^{-1}, \tag{7}$$

where $\hat{Q} = \langle\{\hat{X}_{i\sigma}, \hat{X}^{\dagger}_{i\sigma}\}\rangle = \begin{pmatrix} Q_2 & 0 \\ 0 & Q_1 \end{pmatrix}$. The weight factors $Q_2 = \langle X_i^{22} + X_i^{\sigma\sigma}\rangle = n/2$ and $Q_1 = \langle X_i^{00} + X_i^{\bar{\sigma}\bar{\sigma}}\rangle = 1 - Q_2$ in a paramagnetic state depend only on the hole occupation number (3). The frequency matrix (7) determines the QP spectra within the generalized mean-field approximation (MFA). The corresponding zero-order GF in MFA reads:

$$\hat{G}^0_{\sigma}(\mathbf{k},\omega) = \left(\omega\hat{\tau}_0 - \hat{\varepsilon}(\mathbf{k})\right)^{-1}\hat{Q}, \tag{8}$$

where $\hat{\tau}_0$ is the unity matrix, and we introduced the frequency matrix (7) in the k-representation $\hat{\varepsilon}(\mathbf{k})$. By differentiating the many-particle GF $\langle\langle \hat{Z}^{\rm ir}_{i\sigma}(t) \,|\, \hat{X}^{\dagger}_{j\sigma}(t')\rangle\rangle$ over the second time t' and applying the same projection procedure as in (5) we derive the Dyson equation in the form [15]

$$\hat{G}_{\sigma}(\mathbf{k},\omega)^{-1} = \hat{G}^0_{\sigma}(\mathbf{k},\omega)^{-1} - \hat{\Sigma}_{\sigma}(\mathbf{k},\omega). \tag{9}$$

Here the self-energy matrix $\hat{\Sigma}_{\sigma}(\mathbf{k},\omega)$ is determined by a *proper* part (which have no single zero-order GF) of the many-particle GF in the form

$$\hat{\Sigma}_{\sigma}(\mathbf{k},\omega) = \hat{Q}^{-1}\langle\langle \hat{Z}^{(\rm ir)}_{\sigma} \,|\, \hat{Z}^{(\rm ir)\dagger}_{\sigma}\rangle\rangle^{(\rm prop)}_{\mathbf{k},\omega}\, \hat{Q}^{-1}. \tag{10}$$

Equations (8)–(10) provide an exact representation for the GF (4). However, to calculate it one has to use approximations for the self-energy matrix (10) which describes inelastic scattering of electrons on spin and charge fluctuations.

It is important to point out that contrary to spin-fermion models, where electron interaction with spin- or charge fluctuations are specified by coupling constants, in the Hubbard model these interactions are induced by the kinematic interaction with the coupling constants equal to the original hopping parameters. For instance, the equation of motion for the operator $X_i^{\sigma 2}$ reads

$$\begin{aligned} id\,X_i^{\sigma 2}/dt &= [X_i^{\sigma 2}, H] = (\varepsilon_1 + \Delta)X_i^{\sigma 2} \\ &+ \sum_{l\neq i,\sigma'}\left(t^{22}_{il}B^{22}_{i\sigma\sigma'}X_l^{\sigma' 2} - 2\sigma t^{21}_{il}B^{21}_{i\sigma\sigma'}X_l^{0\bar{\sigma}'}\right) \\ &- \sum_{l\neq i} X_i^{02}\left(t^{11}_{il}X_l^{\sigma 0} + 2\sigma t^{21}_{il}X_l^{2\bar{\sigma}}\right), \end{aligned} \tag{11}$$

where $B^{\alpha\beta}_{i\sigma\sigma'}$ are Bose-like operators describing the number (charge) and spin fluctuations:

$$\begin{aligned} B^{22}_{i\sigma\sigma'} &= (X_i^{22} + X_i^{\sigma\sigma})\delta_{\sigma'\sigma} + X_i^{\sigma\bar{\sigma}}\delta_{\sigma'\bar{\sigma}} \\ &= (N_i/2 + S_i^z)\delta_{\sigma'\sigma} + S_i^{\sigma}\delta_{\sigma'\bar{\sigma}}, \\ B^{21}_{i\sigma\sigma'} &= (N_i/2 + S_i^z)\delta_{\sigma'\sigma} - S_i^{\sigma}\delta_{\sigma'\bar{\sigma}}. \end{aligned} \tag{12}$$

Therefore, in the Hubbard model (1) we have no fitting parameters for electron interaction with spin- or charge fluctuations.

2.2. Mean-Field Approximation. The single-particle excitations in MFA are defined by the frequency matrix (7). By using equations of motion like (11), we get the following energy spectrum for holes in two subbands:

$$\begin{aligned} \varepsilon_{1,2}(\mathbf{k}) &= (1/2)[\omega_2(\mathbf{k}) + \omega_1(\mathbf{k})] \mp (1/2)\Lambda(\mathbf{k}), \\ \Lambda(\mathbf{k}) &= \{[\omega_2(\mathbf{k}) - \omega_1(\mathbf{k})]^2 + 4W(\mathbf{k})^2\}^{1/2}, \end{aligned} \tag{13}$$

where the original excitation spectra in the Hubbard subbands and the hybridization parameter are

$$\begin{aligned} \omega_1(\mathbf{k}) &= 4t\,\alpha_1\gamma(\mathbf{k}) + 4t'\,\beta_1\gamma'(\mathbf{k}) - \mu, \\ \omega_2(\mathbf{k}) &= 4t\,\alpha_2\gamma(\mathbf{k}) + 4t'\,\beta_2\gamma'(\mathbf{k}) + \Delta - \mu, \\ W(\mathbf{k}) &= 4t\,\alpha_{12}\gamma(\mathbf{k}) + 4t'\,\beta_{12}\gamma'(\mathbf{k}), \end{aligned} \tag{14}$$

where we omitted t'' contribution in (2) and introduced the renormalization parameters $\alpha_{1(2)} = Q_{1(2)}[1 + C_1/Q^2_{1(2)}]$, $\beta_{1(2)} = Q_{1(2)}[1 + C_2/Q^2_{1(2)}]$, $\alpha_{12} = \sqrt{Q_1Q_2}[1 - C_1/Q_1Q_2]$, $\beta_{12} = \sqrt{Q_1Q_2}[1 - C_2/Q_1Q_2]$. As in the Hubbard I approximation, we neglect number fluctuations $\langle\delta N_i\delta N_j\rangle_{(i\neq j)}$ but take into account contributions from the spin correlation functions for the n.n. and the n.n.n. sites:

$$C_1 = \langle \mathbf{S}_i\mathbf{S}_{i\pm a_x/a_y}\rangle, \quad C_2 = \langle \mathbf{S}_i\mathbf{S}_{i\pm a_x\pm a_y}\rangle. \tag{15}$$

For the diagonal components of the zero-order GF (8) we have

$$G^0_{11(22)}(\mathbf{k},\omega) = \frac{Q_{1(2)}\,[1 - b(\mathbf{k})]}{\omega - \varepsilon_{1(2)}(\mathbf{k})} + \frac{Q_{1(2)}\,b(\mathbf{k})}{\omega - \varepsilon_{2(1)}(\mathbf{k})}, \tag{16}$$

where the parameter

$$b(\mathbf{k}) = \frac{\varepsilon_2(\mathbf{k}) - \omega_2(\mathbf{k})}{\varepsilon_2(\mathbf{k}) - \varepsilon_1(\mathbf{k})} = \frac{1}{2} - \frac{\omega_2(\mathbf{k}) - \omega_1(\mathbf{k})}{2\Lambda(\mathbf{k})} \tag{17}$$

determines the contribution due to the hybridization.

2.3. Self-Energy Corrections. Dyson equation (9) for the GF is convenient to write in the form

$$\hat{G}_{\sigma}(\mathbf{k},\omega) = \left(\omega\hat{\tau}_0 - \hat{\varepsilon}(\mathbf{k}) - \tilde{\Sigma}_{\sigma}(\mathbf{k},\omega)\right)^{-1}\hat{Q}, \tag{18}$$

where the self-energy reads

$$\tilde{\Sigma}_{\sigma}(\mathbf{k},\omega) = \langle\langle \hat{Z}^{(\rm ir)}_{\sigma} \,|\, \hat{Z}^{(\rm ir)\dagger}_{\sigma}\rangle\rangle^{(\rm prop)}_{\mathbf{k},\omega}\, \hat{Q}^{-1}. \tag{19}$$

To make the problem tractable, we can neglect in the self-energy matrix (19) the off-diagonal components $\tilde{\Sigma}_{12,\sigma}(\mathbf{k},\omega)$ in comparison with the hybridization parameters $W(\mathbf{k})$ in (14). This enables us to write the diagonal components of the full GF (18) in the form similar to (16)

$$\hat{G}_{11(22)}(\mathbf{k},\omega) = \frac{Q_{1(2)}\,[1-b(\mathbf{k})]}{\omega-\varepsilon_{1(2)}(\mathbf{k})-\tilde{\Sigma}_{11(22)}(\mathbf{k},\omega)} + \frac{Q_{1(2)}\,b(\mathbf{k})}{\omega-\varepsilon_{2(1)}(\mathbf{k})-\tilde{\Sigma}_{22(11)}(\mathbf{k},\omega)}. \tag{20}$$

Here the hybridization parameters $b(\mathbf{k})$ are determined by the formula similar to (17) which gives an accurate approximation for a small doping at $n \sim 1$.

Now we calculate the self-energy (19) in the non-crossing (NCA) or the self-consistent Born approximation (SCBA) by neglecting vertex renormalization. As follows from the equation of motion (11), the $\hat{Z}_\sigma^{(\mathrm{ir})}$ operators determined by (5) are essentially a product of the Fermi-like $X_j(t)$ and Bose-like $B_i(t)$ operators. In SCBA, the propagation of these excitations of different types in the many-particle GF in (19) are assumed to be independent of each other. Therefore, they can be decoupled in the time-dependent correlation functions for lattice sites ($i \neq j$, $l \neq m$) as follows:

$$\langle B_i(t)X_j(t)B_l(t')X_m(t')\rangle \simeq \langle X_j(t)X_m(t')\rangle\langle B_i(t)B_l(t')\rangle. \tag{21}$$

Using the spectral representation for these correlation functions, we obtain the following formula for the diagonal self-energy components $\tilde{\Sigma}_{11(22)}(\mathbf{k},\omega) = \Sigma(\mathbf{k},\omega)$ which are the same for two subbands:

$$\Sigma(\mathbf{k},\omega) = \frac{1}{N}\sum_{\mathbf{q}}\int_{-\infty}^{+\infty} dz K(\omega,z|\mathbf{q},\mathbf{k}-\mathbf{q}) \times (-1/\pi)\,\mathrm{Im}\,[G_1(\mathbf{q},z)+G_2(\mathbf{q},z)], \tag{22}$$

where the corresponding subband GFs are

$$G_{1(2)}(\mathbf{q},\omega) = \frac{1}{\omega-\varepsilon_{1(2)}(\mathbf{q})-\Sigma(\mathbf{q},\omega)}. \tag{23}$$

The kernel of the integral equation (22) has a form, similar to the strong coupling Migdal–Eliashberg theory [21,22]:

$$K(\omega,z|\mathbf{q},\mathbf{k}-\mathbf{q}) = |t(\mathbf{q})|^2\,\frac{1}{2\pi}\int_{-\infty}^{+\infty}\frac{d\Omega}{\omega-z-\Omega} \times [\tanh(z/2T)+\coth(\Omega/2T)]\,\mathrm{Im}\,\chi_{sc}(\mathbf{k}-\mathbf{q},\Omega), \tag{24}$$

where the interaction is defined by the hopping parameter $t(\mathbf{q})$ (2). The spectral density of bosonic excitations is determined by the dynamic susceptibility of the Bose-like operators $B_i(t)$ in (21) — the spin and number (charge) fluctuations

$$\chi_{sc}(\mathbf{q},\omega) = -[\langle\langle \mathbf{S}_\mathbf{q}|\mathbf{S}_{-\mathbf{q}}\rangle\rangle_\omega + (1/4)\langle\langle \delta N_\mathbf{q}|\delta N_{-\mathbf{q}}\rangle\rangle_\omega], \tag{25}$$

where we introduced the commutator GF for the spin $\mathbf{S}_\mathbf{q}$ and the number $\delta N_\mathbf{q} = N_\mathbf{q} - \langle N_\mathbf{q}\rangle$ operators.

Thus we obtain a self-consistent system of equations for the GFs (23) and the self-energy (22). A similar system of equations was obtained within the composite operator method [13]. In comparison with the t–J model studied by us in [16], for the Hubbard model (1) we have two contributions in the self-energy (22) determined by the two Hubbard subbands, while in the t–J model only one subband is considered. However, depending on the position of the chemical potential, a substantial contribution to the self-energy comes only from the GF of those subband which is close to the Fermi energy. A contribution from the GF of another subband which is far from the Fermi energy, is suppressed due to a large charge-transfer energy Δ in the denominator of those GF. Neglecting the latter contribution, we obtain a self-consistent system of equations for one GF close to the Fermi energy and the corresponding self-energy function similar to the t–J model [16].

3. RESULTS AND DISCUSSION

3.1. Self-Consistent System of Equations. To solve the system of equations for the self-energy (22) and the GFs (23) we should specify a model for the spin-charge susceptibility (25). Below we take into account only the spin-fluctuation contribution $\chi_s(\mathbf{q},\omega) = -\langle\langle \mathbf{S}_q \mid \mathbf{S}_{-q}\rangle\rangle_\omega$ for which we adopt a model suggested in numerical studies [23]

$$\mathrm{Im}\,\chi_s(\mathbf{q},\omega+i0^+) = \chi_s(\mathbf{q})\,\chi_s''(\omega) = \frac{\chi_0}{1+\xi^2(1+\gamma(\mathbf{q}))}\,\tanh\frac{\omega}{2T}\,\frac{1}{1+(\omega/\omega_s)^2}. \tag{26}$$

We stress that we consider the model for spin-fluctuation spectrum $\chi_s''(\omega)$ in the form of a continuum characterized by the spin-fluctuation energy $\omega_s \simeq J$ of the order of the exchange energy $J = 0.4t$. The $\mathbf{q}$-dependence in $\chi_s(\mathbf{q})$ is determined by the AF correlation length ξ which doping dependence is defined below. The coupling constant χ_0 at the AF wave vector $\mathbf{Q} = (\pi,\pi)$ is fixed by the normalization condition

Table 1. Static spin correlation functions (29), $C(\xi)$ (30) and the AF correlation length ξ (26) at various hole concentrations $n = 1 + \delta$

$\delta =$	0.03	0.05	0.10	0.15	0.20	0.30
C_1	–0.36	–0.26	–0.21	–0.18	–0.14	–0.10
C_2	0.27	0.16	0.11	0.09	0.06	0.04
$C(\xi)$	22.0	5.91	3.58	2.67	1.93	1.40
ξ	8.0	3.40	2.50	2.10	1.70	1.40

$$\frac{1}{N}\sum_i \langle \mathbf{S}_i \mathbf{S}_i \rangle = \frac{3}{4}\langle (1 - X_i^{00} - X_i^{22}) \rangle = \frac{3}{4}(1 - |\delta|)$$

$$= \frac{1}{\pi}\int_{-\infty}^{+\infty} \frac{dz}{\exp(z/T) - 1} \chi_s''(z)\, \frac{1}{N}\sum_{\mathbf{q}} \chi_s(\mathbf{q}), \tag{27}$$

which gives the following value for the coupling constant:

$$\chi_0 = \frac{3(1 - |\delta|)}{2\,\omega_s} \left\{ \frac{1}{N}\sum_{\mathbf{q}} \frac{1}{1 + \xi^2[1 + \gamma(\mathbf{q})]} \right\}^{-1}. \tag{28}$$

In (27) for the hole concentration $\delta = 1 - n = \langle X_i^{22} - X_i^{00} \rangle$ we assume that at the hole doping $\delta = \langle X_i^{22} \rangle$ at $\langle X_i^{00} \rangle = 0$, while at the electron doping $\delta = -\langle X_i^{00} \rangle$ at $\langle X_i^{22} \rangle = 0$ which is reasonable for small $|\delta|$.

The spin correlation functions (15) in the single-particle excitation spectra (13) in MFA are defined by the equations

$$C_1 = \frac{1}{N}\sum_{\mathbf{q}} C_{\mathbf{q}}\, \gamma(\mathbf{q}), \quad C_2 = \frac{1}{N}\sum_{\mathbf{q}} C_{\mathbf{q}}\, \gamma'(\mathbf{q}). \tag{29}$$

The static correlation function $C_{\mathbf{q}}$ can be calculated from the same model (26) as follows:

$$C_{\mathbf{q}} = \langle \mathbf{S}_{\mathbf{q}} \mathbf{S}_{-\mathbf{q}} \rangle = \frac{C(\xi)}{1 + \xi^2[1 + \gamma(\mathbf{q})]}, \tag{30}$$

where the factor $C(\xi) = \chi_0\,(\omega_s/2)$.

To specify the doping dependence of the AF correlation length $\xi(\delta)$ at low temperature, we fit the correlation function C_1 calculated from (29) to the numerical results of an exact diagonalization for finite clusters [24]. The values of the AF correlation length, calculated values of C_2 and the correlation function $C(\xi) = \langle \mathbf{S}_{\mathbf{q}} \mathbf{S}_{-\mathbf{q}} \rangle$ at the AF wave vector $\mathbf{q} = \mathbf{Q} = (\pi, \pi)$ are given in Table 1.

To perform numerical calculations, we introduce the imaginary frequency representation for the GF (23):

$$G_{1(2)}(\mathbf{q}, i\omega_n) = \frac{1}{i\omega_n - \varepsilon_{1(2)}(\mathbf{q}) - \Sigma(\mathbf{q}, i\omega_n)}, \tag{31}$$

where $i\omega_n = i\pi T(2n + 1)$, $n = 0, \pm 1, \pm 2, \ldots$ For the self-energy (22) we obtain the following representation:

$$\Sigma(\mathbf{k}, i\omega_n) = -\frac{T}{N}\sum_{\mathbf{q}}\sum_m [G_1(\mathbf{q}, i\omega_m) + G_2(\mathbf{q}, i\omega_m)]$$
$$\times\ \lambda(\mathbf{q}, \mathbf{k} - \mathbf{q} \mid i\omega_n - i\omega_m). \tag{32}$$

The interaction function is given here by the equation

$$\lambda(\mathbf{q}, \mathbf{k} - \mathbf{q} \mid i\omega_\nu) = -|t(\mathbf{q})|^2\, \chi_s(\mathbf{q})\, F_s(i\omega_\nu), \tag{33}$$

where the spectral function

$$F_s(\omega_\nu) = \frac{1}{\pi}\int_0^\infty \frac{2x\,dx}{x^2 + (\omega_\nu/\omega_s)^2} \frac{1}{1 + x^2} \tanh\frac{x\,\omega_s}{2T}. \tag{34}$$

In the next sections we consider the results of self-consistent calculations of the GFs (31) and the self-energy (32) in the hole-doped case for various hole concentrations $\delta = n - 1 > 0$. In Subsecs. 3.2–3.4 the calculations were performed at temperature $T = 0.03t \simeq 140$ K and $T = 0.3t$ for $\Delta = 8t$, $t \simeq 0.4$ eV and $t' = -0.3t$. Several results are reported for $\Delta = 4t$, $t' = -0.13t$, $t'' = 0.16t$ in Subsec. 3.5. For the spin-fluctuation energy in (26) we take $\omega_s = 0.4t$. The AF correlation length $\xi(\delta)$ and the static correlation functions C_1, C_2 in (15) are defined in Table 1.

3.2. Dispersion and Spectral Functions. In ARPES measurements and QMC simulations the spectrum of single-electron excitations is determined by the spectral function $A_{(\mathrm{el})}(\mathbf{k}, \omega) = A_{(\mathrm{h})}(\mathbf{k}, -\omega)$. The spectral function for holes can be written as follows:

$$A_{(\mathrm{h})}(\mathbf{k}, \omega) = -\frac{1}{\pi}\,\mathrm{Im}\,\langle\langle a_{\mathbf{k}\sigma} \mid a_{\mathbf{k}\sigma}^\dagger \rangle\rangle_{\omega + i0^+}$$
$$= [Q_1 + P(\mathbf{k})]A_1(\mathbf{k}, \omega) + [Q_2 - P(\mathbf{k})]A_2(\mathbf{k}, \omega). \tag{35}$$

Here we introduced for the hole annihilation $a_{\mathbf{k}\sigma}$ and creation $a_{\mathbf{k}\sigma}^\dagger$ operators the definition in terms of the Hubbard operators $a_{\mathbf{k}\sigma} = X_i^{0\sigma} + 2\sigma X_i^{\bar{\sigma}2}$, $a_{\mathbf{k}\sigma}^\dagger = X_i^{\sigma 0} + 2\sigma X_i^{2\bar{\sigma}}$ and used all four components of the matrix GF (18) $\hat{G}_{\alpha\beta}(\mathbf{k}, \omega)$ with the diagonal components given by (20). In (35) we introduced also the

one-band spectral functions determined by the GFs (23): $A_{1(2)}(\mathbf{k},\omega) = -(1/\pi)\,\mathrm{Im}G_{1(2)}(\mathbf{q},\omega)$. The hybridization effects are allowed for by the parameter $P(\mathbf{k}) = (n-1)b(\mathbf{k}) - 2\sqrt{Q_1 Q_2}\,W(\mathbf{k})/\Lambda(\mathbf{k})$.

The dispersion curves given by maxima of spectral functions (35) were calculated for hole doping $\delta = 0.05 - 0.3$. At low hole doping, $\delta = 0.05$, 0.1, the dispersion reveals a rather flat hole-doped band at the Fermi energy (FE) ($\omega = 0$) as shown in the left panels in Fig. 1 and Fig. 2. The corresponding spectral function (the right panels) demonstrates weak QP peaks at the Fermi energy. With doping, the dispersion and the intensity of the QP peaks at the Fermi

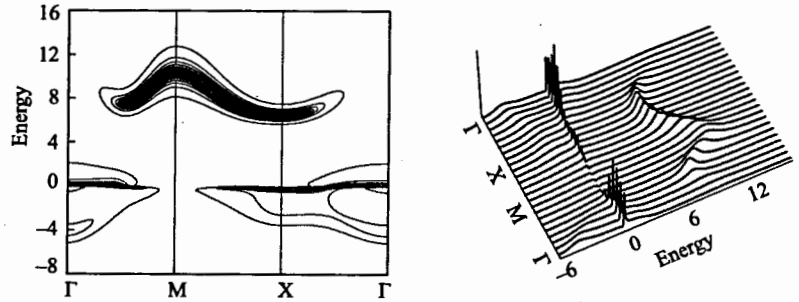

Fig. 1. Dispersion curves (left panel) and spectral functions (right panel) in units of t along the symmetry directions $\Gamma(0,0) \to M(\pi,\pi) \to X(\pi,0) \to \Gamma(0,0)$ for $\delta = 0.05$

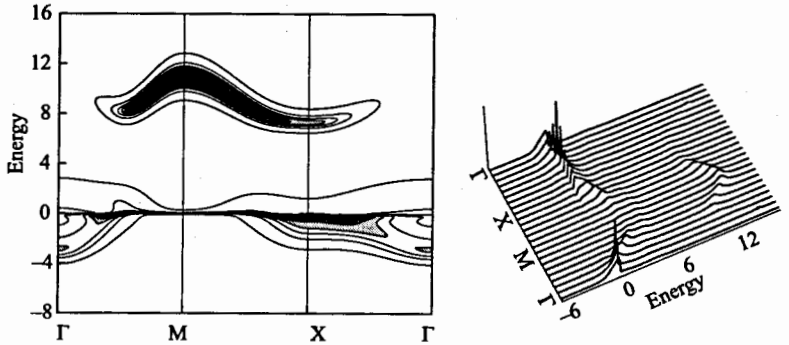

Fig. 2. The same as in Fig. 1, for $\delta = 0.1$

energy substantially increase as demonstrated in Fig. 3 and Fig. 4 though a flat band in $X(\pi,0) \to \Gamma(0,0)$ direction is still observed in accordance with ARPES measurements in the overdoped $La_{1.78}Sr_{0.22}CuO_4$ [25]. To study an influence of AF spin correlations on the spectra, we calculate the spectral functions at high temperature $T = 0.3t$ for $\delta = 0.1$ by neglecting spin correlation functions (15)

in the single-particle excitation spectra (13) in MFA and taking a small AF correlation length ($\xi = 1.0$) in the spin-susceptibility (26). Figure 5 shows a strong increase of the dispersion and the intensity of the QP peaks at the Fermi energy as in the overdoped region, $\delta = 0.3$, which proves a strong influence of AF spin correlations on the spectra. A crude estimation of the Fermi velocity from

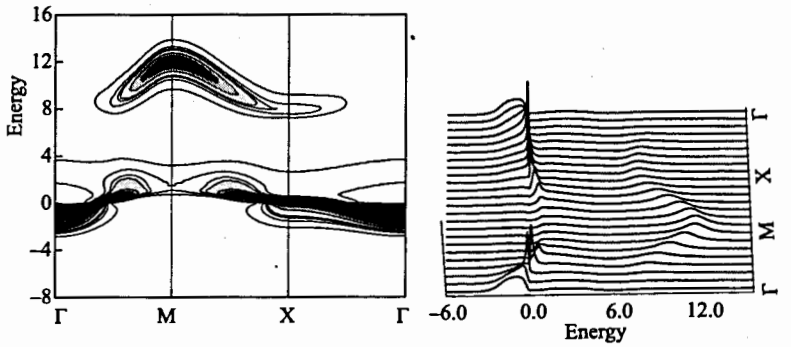

Fig. 3. The same as in Fig. 1, for hole concentration $\delta = 0.2$

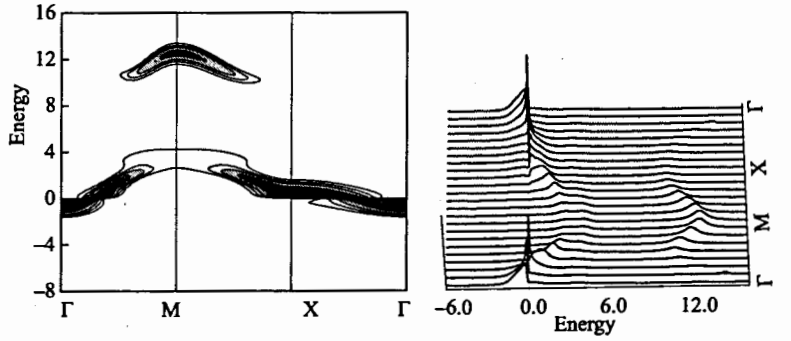

Fig. 4. The same as in Fig. 1, for hole concentration $\delta = 0.3$

the dispersion curve in the $\Gamma(0,0) \to M(\pi,\pi)$ direction in Fig. 4 for the overdoped case gives the value $V_F \simeq 7.5t$ Å $\simeq 3$ (eV·Å) for the hopping parameter $t = 0.4$ eV which can be compared with experimental results $V_F \simeq 2.2$ (eV·Å) for overdoped $La_{1.78}Sr_{0.22}CuO_4$ [25] and $V_F \simeq 3.9$ (eV·Å) for overdoped Bi-2212 [26]. With doping, the electronic density of states (DOS) shows a weight transfer from the upper one-hole subband to the lower two-hole singlet subband as shown in Fig. 6 (left panel). However, even in the overdoped case a noticeable part of the DOS retains in the upper one-hole subband.

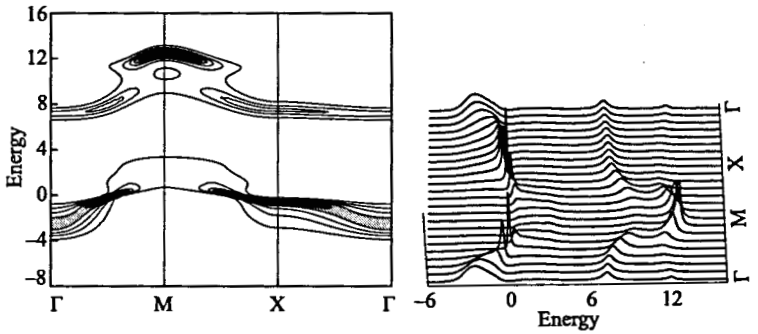

Fig. 5. The same as in Fig. 1, for hole concentration $\delta = 0.1$ but at high temperature $T = 0.3t$

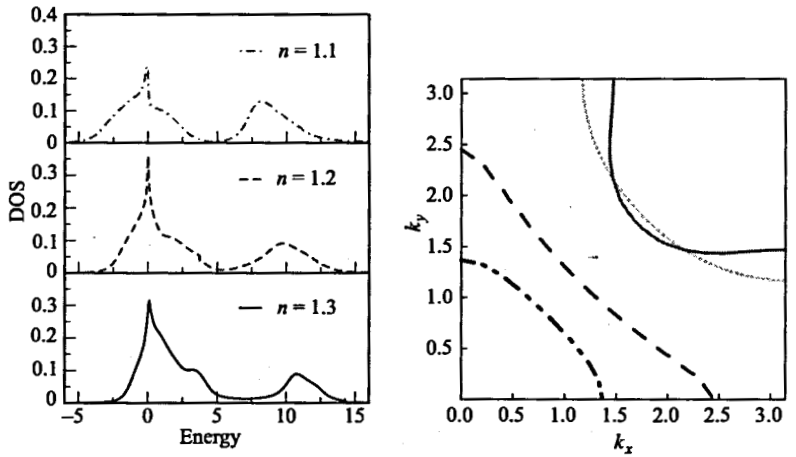

Fig. 6. Doping dependence of the DOS (left panel) and FS for $\delta = 0.1$ (solid line at $T = 0.03t$ and dotted line at $T = 0.3t$), $\delta = 0.2$ (dashed line), and $\delta = 0.3$ (dot-dashed line) (right panel)

3.3. Fermi Surface and Occupation Numbers. The Fermi surface for the two-hole subband was determined by a conventional equation: $\varepsilon_2(\mathbf{k_F}) + \mathrm{Re}\,\Sigma(\mathbf{k_F}, \omega = 0) = 0$ (Fig. 6) (right panel) and then compared with those one obtained from maxima of the spectral function $A_{\mathrm{el}}(\mathbf{k}, \omega = 0)$ on the (k_x, k_y)-plane for $\delta = 0.1$, 0.2, 0.3 shown in Fig. 7. The FS changes from a hole arc-type at $\delta = 0.1$ to an electron-like one at $\delta = 0.3$. Experimentally an electron-like FS was observed in the overdoped $La_{1.78}Sr_{0.22}CuO_4$ [25]. The doping-dependent FS transformation can be also observed by studying the electron occupation numbers. The electron occupation numbers in (k)-space for one-spin direction equal to $N_{(\mathrm{el})}(\sigma, \mathbf{k}) = 1 - N_{(\mathrm{h})}(\sigma, \mathbf{k})$ where the hole occupation numbers

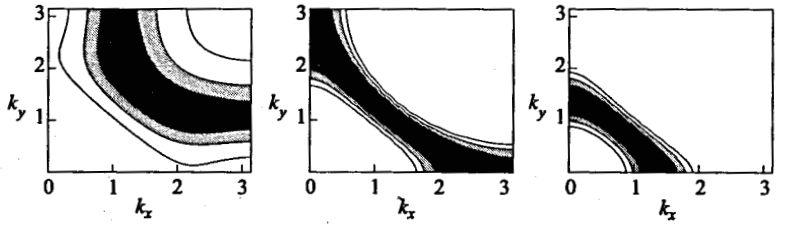

Fig. 7. $A(\mathbf{k}, \omega = 0)$ on the FS for $\delta = 0.1$ (left panel), $\delta = 0.2$ (central panel), and $\delta = 0.3$ (right panel)

$N_{(\mathrm{h})}(\sigma, \mathbf{k}) \equiv N_{(\mathrm{h})}(\mathbf{k})$ according to (3) are determined only by the diagonal GFs (20). From the latter equation and (23) we get

$$
\begin{aligned}
N_{(\mathrm{h})}(\mathbf{k}) &= [Q_1 + (n-1)b(\mathbf{k})]\, N_1(\mathbf{k}) \\
&+ [Q_2 - (n-1)b(\mathbf{k})\, N_2(\mathbf{k}), \\
N_{1(2)}(\mathbf{k}) &= -\frac{1}{\pi} \int_{-\infty}^{\infty} \frac{d\omega}{e^{\omega/T} + 1}\, \mathrm{Im}\, G_{1(2)}(\mathbf{k}, \omega) \\
&= \frac{1}{2} + \frac{T}{2} \sum_{m=-\infty}^{\infty} G_{1(2)}(\mathbf{k}, i\omega_m). \qquad (36)
\end{aligned}
$$

The electron occupation numbers in a quarter of the BZ $(0 < k_x, k_y < \pi)$ are shown in Fig. 8 for $\delta = 0.1$ at low temperature $T = 0.03t$ and at high temperature $T = 0.3t$. With doping the shape of the $N_{\mathbf{k}}$ is changing revealing a transition of the hole-like FS to the electron-like ones in the overdoped case $\delta = 0.3$ as plotted in Fig. 9. While in the underdoped case at $\delta = 0.1$, the drop of the

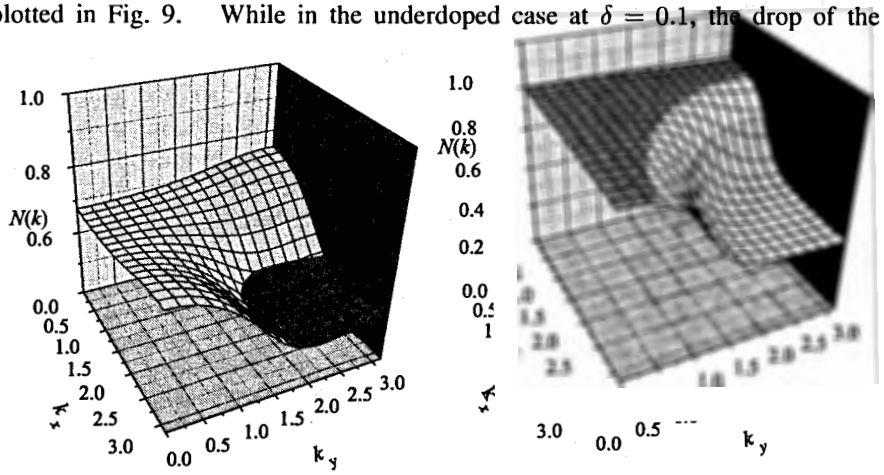

Fig. 8. The electronic occupation numbers $N_{\mathbf{k}}$ for $\delta = 0.1$ at $T = 0.03t$ (left panel) and at $T = 0.3t$ (right panel)

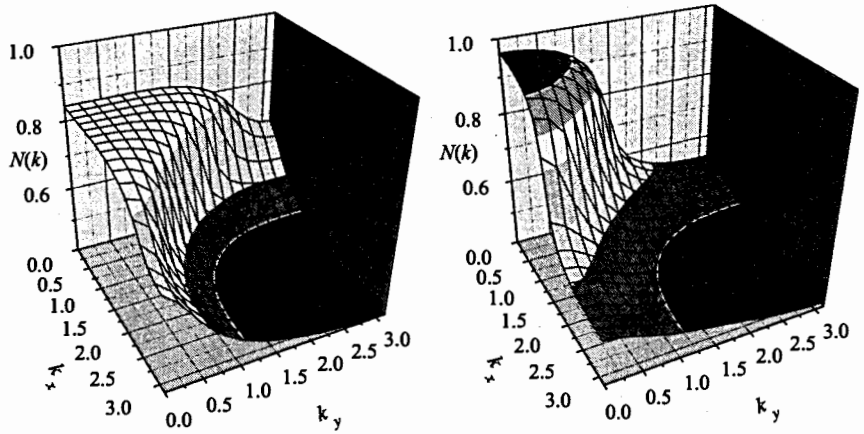

Fig. 9. The electronic occupation numbers $N_{\mathbf{k}}$ at $T = 0.03t$ for $\delta = 0.2$ (left panel) and at $\delta = 0.3$ (right panel)

occupation numbers at the Fermi level crossing is rather small, $\Delta N_{(\mathrm{el})} \simeq 0.15$, for high temperature $T = 0.3t$ or in the overdoped case at $\delta = 0.3$ when the AF spin correlations are suppressed, the occupation number drops are substantially increased: $\Delta N_{(\mathrm{el})} \simeq 0.45$, 0.55, respectively. Thus, the arc formation and a small change of the electron occupation numbers at the FS crossing at low doping further prove a large contribution of the spin correlations in the renormalization of QP spectra.

3.4. Self-Energy and Kinks. Energy dependence of the real and imaginary parts of the self-energy $\Sigma(\mathbf{k},\omega)$ for $\delta = 0.1$, 0.2, 0.3 at the $\Gamma(0,0)$, $S(\pi/2,\pi/2)$ and $M(\pi,\pi)$ points are shown in Fig. 10 and Fig. 11. These plots demonstrate a strong dependence of the self-energy on the wave-vector and the hole concentrations. With doping, the coupling constant substantially decreases as is seen by the decreasing of the imaginary part and the slope of the real part at the FS crossing which determines the coupling constant $\lambda = -(\partial \mathrm{Re}\tilde{\Sigma}(\mathbf{k},\omega)/\partial\omega)_{\omega=0}$. As shown in Fig. 11 (right panel), the coupling constant decreases from $\lambda \simeq 7.86$ at $\delta = 0.1$ to $\lambda \simeq 3.3$ at $\delta = 0.3$.

At large binding energies (greater than the boson energy responsible for the interaction) the self-energy effects vanish and the electron dispersion should return to the bare value, giving a sharp bend, the so-called «kink» in the electron dispersion. The amplitude of the kink and the energy scale where it occurs are related to the strength of the electron–boson interaction and the boson energy, respectively. In ARPES the kink is observed as a changing of the slope for an intensity plot for the spectral function $A(\mathbf{k},\omega)$ in a particular k-wave vector direction below the Fermi level $\omega \leqslant 0$ (for electrons). Usually, two directions

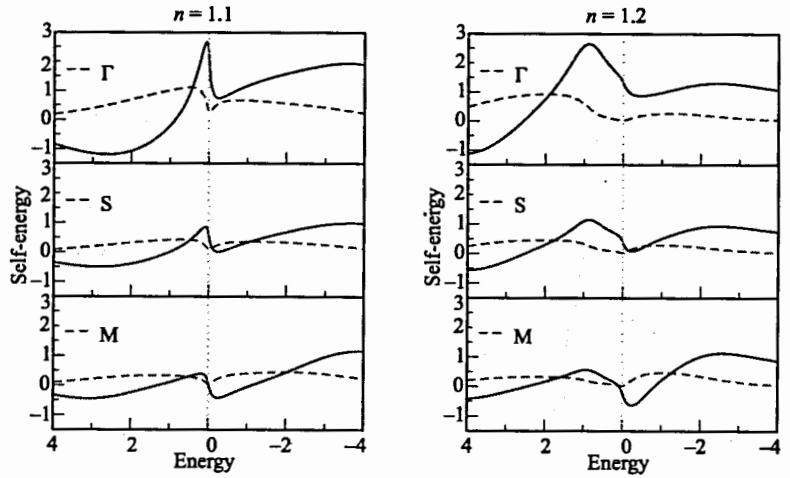

Fig. 10. Energy dependence of the real and imaginary parts of the self-energy $\Sigma(\mathbf{k},\omega)$ at the $\Gamma(0,0)$, $S(\pi/2,\pi/2)$ and $M(\pi,\pi)$ points at $\delta = 0.1$ (left panel) and $\delta = 0.2$ (right panel)

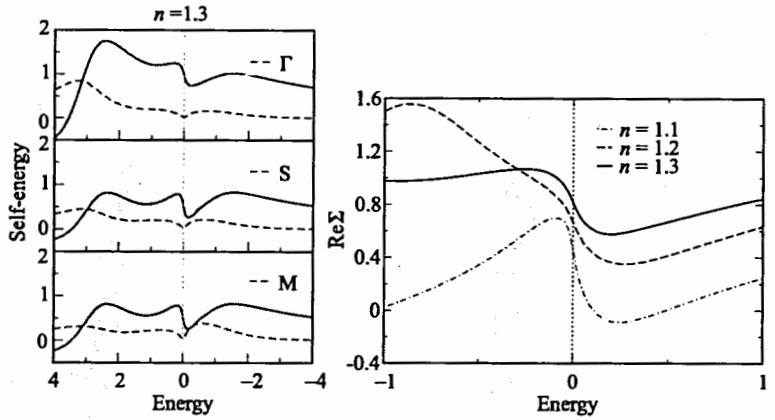

Fig. 11. The same as in Fig. 10, for hole concentration $\delta = 0.3$ (left panel) and $\mathrm{Re}\Sigma(\mathbf{k},\omega)$ at the FS (right panel)

are studied: the nodal ($\Gamma \to M$) and the antinodal ($X \to M$). Intensity plots for the spectral function $A(\mathbf{k},\omega)$ at $\delta = 0.1$ are shown in Fig. 12 in the nodal direction (left panel) and the antinodal one (right panel). The same plots at $\delta = 0.3$ are shown in Fig. 13 in the nodal direction (left panel) and the antinodal $X(\pi,0) \to \Gamma(0,0)$ direction (right panel). A change of dispersion is clearly seen with increasing binding energy below the FS shown by dotted line. For the

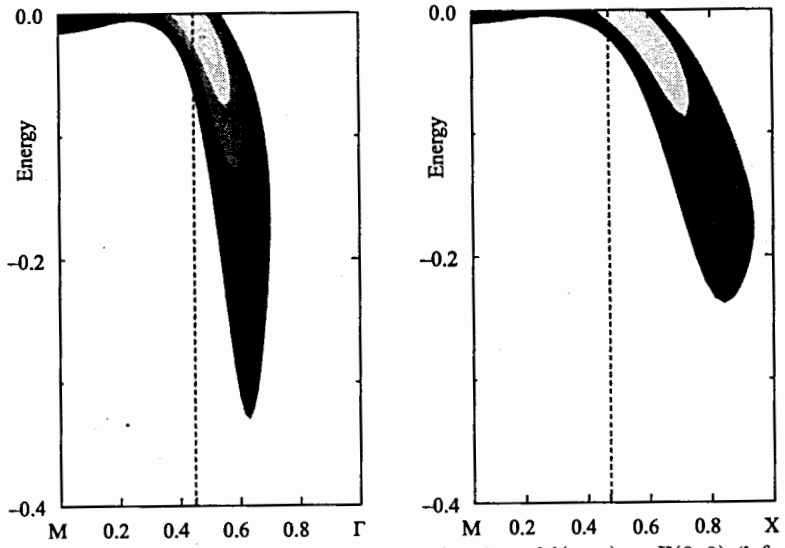

Fig. 12. Dispersion curves along the symmetry directions $M(\pi,\pi) \to \Gamma(0,0)$ (left panel) and $M(\pi,\pi) \to X(\pi,0)$ (right panel) in units of t for $\delta = 0.1$, $T = 0.03t$. Fermi level crossing is shown by vertical dotted line

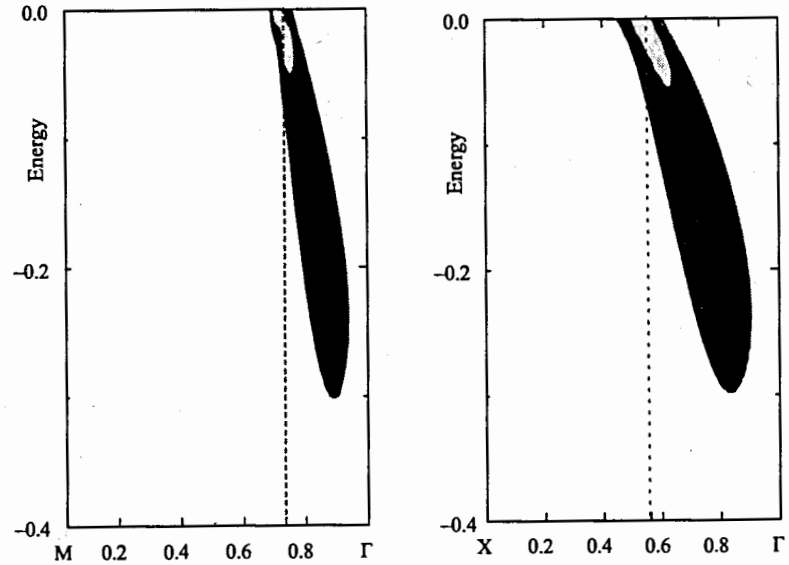

Fig. 13. The same as in Fig. 12 but for $\delta = 0.3$ along the symmetry directions $M(\pi,\pi) \to \Gamma(0,0)$ (left panel) and $X(\pi,0) \to \Gamma(0,0)$ (right panel)

underdoped case the kink is larger than for the overdoped one. A crude estimation of the strength of the kink from the ratio of the dispersion slope $V_{\rm F}$ close to the FS ($\omega = 0$) to those one $V_{\rm F}^0$ at large binding energy ($\omega \sim 0.2t$), $V_{\rm F}^0/V_{\rm F} = (1+\lambda)$, gives the following values: $(1+\lambda) \sim 7.6, 3.5$ at $\delta = 0.1$ for the nodal and antinodal directions, respectively. In the overdoped case the nodal value is much smaller, while in the the antinodal $X(\pi,0) \to \Gamma(0,0)$ direction is still quite large: $(1+\lambda) \sim 2.5$. These estimations are in accord with the evaluation of the coupling constant λ from the slope of the real part of the self-energy discussed above.

It is important to stress that in our theory the self-energy effects and the corresponding kinks are induced by the spin-fluctuation spectrum in the form of the continuum (26) which at low temperature $T \sim 0.03t \ll \omega_s = 0.4t$ has a large intensity already at small energy $\omega \sim 0.03t$ and decreases slowly up to a high energy $\omega \sim t$. In the spin-fermion model the kink phenomenon is usually explained by electron interaction with the spin-resonance mode $\Omega_{\rm res} \simeq 40$ meV which results in a break of the electron dispersion («kink») at a certain energy $\omega \sim \Omega_{\rm res} + \Delta_0$, where Δ_0 is the superconducting gap (see, e. g., [2]). However, the intensity of the spin-resonance mode amounts only few percents of the total spin-fluctuation spectrum given by the sum rule (27) and its consideration should not change our results which reveal a rather strong interaction with a smooth energy variation without any specific kink energy.

3.5. Dispersion and FS at $\mathbf{U_{eff} = \Delta = 4t}$. The effective Coulomb energy in the Hubbard model (1) $U_{\rm eff} = 8t$ results in a large charge-transfer gap $\Delta \simeq 3$ eV for $t = 0.4$ eV even in the overdoped case (Fig. 4) while experiments point to a smaller value of the order of $1.5-2$ eV. To correct this inconsistency, we present in this section the results obtained for a smaller value of $U_{\rm eff} = \Delta = 4t$. We also take into account the hoping parameter for the n.n.n. $\pm 2a_x, \pm 2a_y$ sites by fixing the parameters in the model dispersion (2) as follows: $t' = -0.13t$, $t'' = 016t$.

Main results for the dispersion and the spectral functions are not changed much in comparison with the previous ones as shown in Fig. 14. Larger hybridization between the subbands at small value of $U_{\rm eff}$ results in increase of the dispersion and the intensity of the upper one-hole subband. This trend is also seen in the DOS in the left panel in Fig. 15 where the gap between the subbands vanishes in the overdoped case at $\delta = 0.3$.

Noticeable changes are observed for the FS shown in Fig. 15 (right panel) and in Fig. 16. In the first plot where the FS was determined by the equation $\varepsilon_2(\mathbf{k}_{\rm F}) + {\rm Re}\,\Sigma(\mathbf{k}_{\rm F}, \omega = 0) = 0$, we see a large pocket at small doping $\delta = 0.1$ which opens with doping or temperature increasing. At the overdoping for $\delta = 0.3$, the FS transforms to the electron-like as in the previous calculations. This transformation is confirmed by calculations of the electron occupation numbers shown in Fig. 17. It should be noted that a pronounced hole pocket in the new set of the model parameters is caused by the t'' contribution which results in a large dispersion in the $(\pi,0) \to (0,\pi)$ direction ($\propto t''(\cos 2k_x + \cos 2k_y)$)

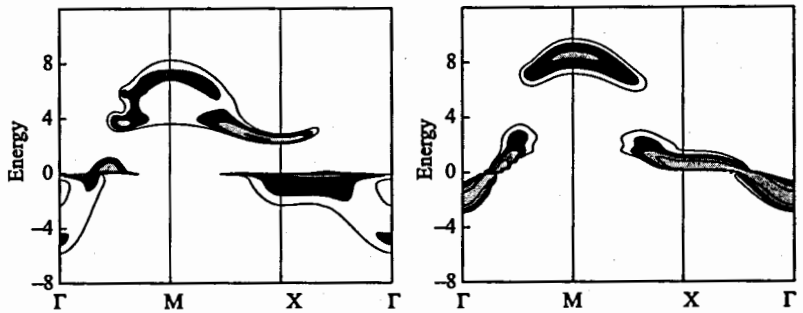

Fig. 14. Dispersion curves for $\Delta = 4t$ along the symmetry directions $\Gamma(0,0) \rightarrow M(\pi,\pi) \rightarrow X(\pi,0) \rightarrow \Gamma(0,0)$ at $\delta = 0.05$ (left panel) and $\delta = 0.3$ (right panel)

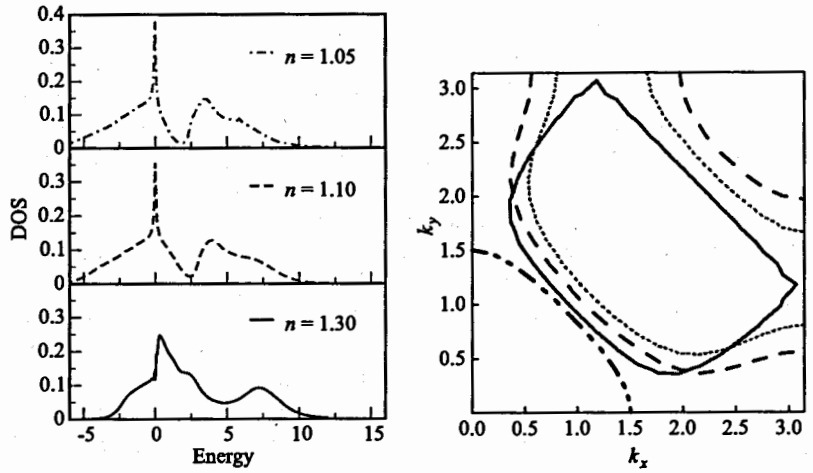

Fig. 15. Doping dependence of the DOS (left panel) and FS for $\delta = 0.1$ (solid line at $T = 0.03t$ and dotted line at $T = 0.3t$), $\delta = 0.2$ (dashed line), and $\delta = 0.3$ (dot-dashed line) (right panel) for $\Delta = 4t$

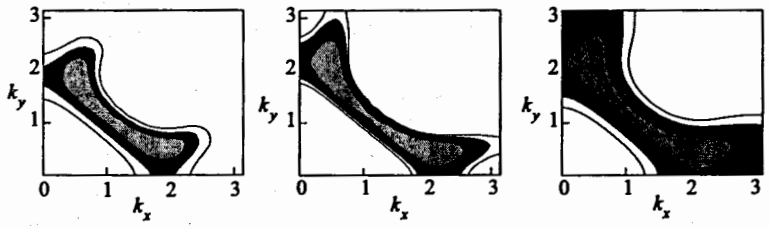

Fig. 16. $A(\mathrm{k},\omega = 0)$ on the FS at $\delta = 0.05$ (left panel) and $\delta = 0.1$ (central panel) at $T = 0.03t$, and $\delta = 0.1$ at $T = 0.3t$ (right panel) for $\Delta = 4t$

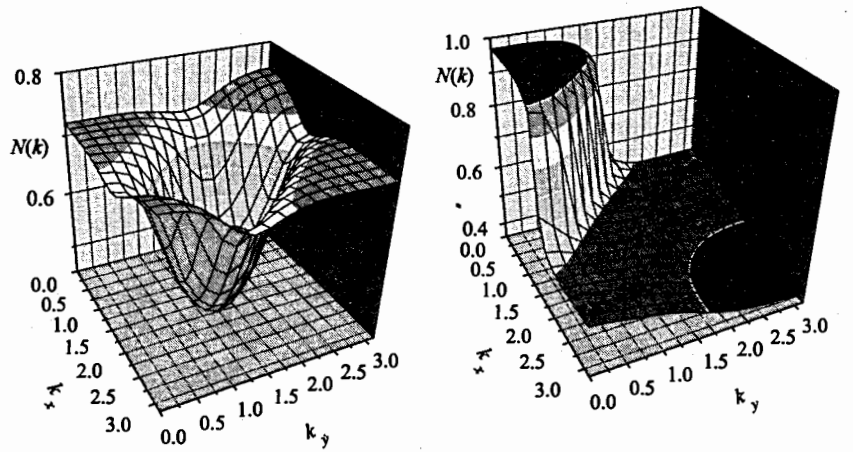

Fig. 17. The electronic occupation numbers N_{k} at $T = 0.03t$ for $\delta = 0.05$ (left panel) and at $\delta = 0.3$ (right panel) for $\Delta = 4t$

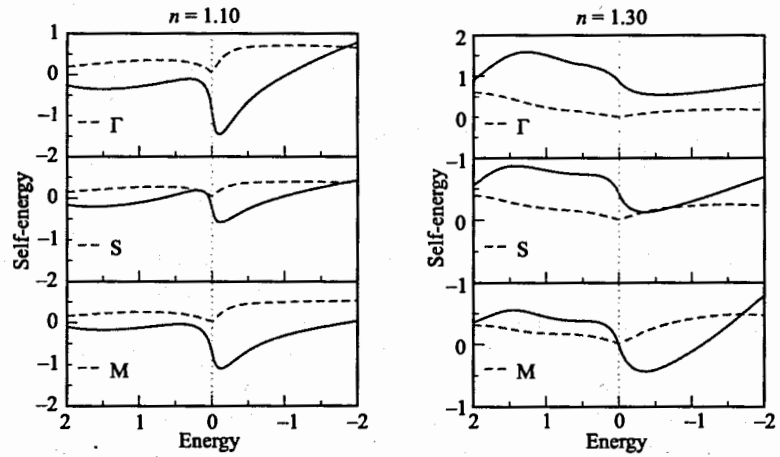

Fig. 18. Energy dependence of the real and imaginary parts of the self-energy $\Sigma(\mathrm{k},\omega)$ for $\Delta = 4t$ at the $\Gamma(0,0)$, $S(\pi/2,\pi/2)$ and $M(\pi,\pi)$ points at $\delta = 0.1$ (left panel) and $\delta = 0.3$ (right panel)

disregarded in the previous set of the parameters. A remarkable feature of these results is that the part of the FS close to the $\Gamma(0,0)$ point in the nodal direction in Fig. 15 does not shift much with doping (or temperature) being pinned to a

large FS as observed in the ARPES experiments (see, e. g., [26]). In fact, only this part of the FS was detected in the ARPES experiments where the spectral function $A_{el}(\mathbf{k}, \omega = 0)$, shown in Fig. 16, was measured.

Concerning the self-energy effects and kinks, they are similar to the case for $\Delta = 8t$ and confirm a strong influence of spin correlations on the QP spectra renormalization. As shown in Fig. 18, the coupling constant $\lambda = -(\partial \mathrm{Re}\tilde{\Sigma}(\mathbf{k}, \omega)/\partial\omega)_{\omega=0}$ being large at small doping distinctly decreases with overdoping at $\delta = 0.3$ accompanied by suppression of the imaginary part of the self-energy. In conclusion, the alternative set of parameters with a moderate effective Coulomb energy $U_{\mathrm{eff}} = 4t$ in the Hubbard model (1) confirms an important role of AF correlations in the electronic structure of system with large single-site Coulomb interaction.

4. CONCLUSION

In the present paper the theory of QP spectra in the strong correlation limit for the Hubbard model (1) in a paramagnetic state is formulated. By employing the Hubbard operator technique in the equation of motion method for the thermodynamic GFs [11], we consistently took into account strong electron correlations and derived the self-consistent system of equation for the GF (23) and the self-energy (22) in the NCA. The latter is equivalent to the Migdal–Eliashberg approximation where the vertex corrections are neglected. This can be justified for a weak coupling. Though in the Hubbard model (1) the electron coupling to the spin-fluctuation scattering is not weak, it is of the order of the hopping parameter t, the vertex corrections should not be so important as for the strong electron–phonon coupling. This is due to the kinematic restrictions of electron scattering on spin fluctuations. As was shown for the t–J model [27], the leading two-loop crossing diagram identically vanishes, while the next three-loop crossing diagram gives a small contribution to the self-energy. In any case, the NCA for the self-energy can be considered as a starting approximation for a model with strong coupling. The most important advantage of our theory is that we have no fitting parameters for the electron interaction with spin fluctuations as in phenomenological approach or spin-fermion models. However, the coupling constant λ for this interaction obtained in our calculations (see Subsec. 3.4) seems to be too large in comparison with the ARPES results. This discrepancy can be caused by disregarding scattering on charge fluctuations in the dynamical susceptibility model (25) and electron–phonon interaction which may reduce electron-spin interaction.

The numerical results for the electron dispersion in Subsec. 3.2, the Fermi surface and the occupation numbers in Subsec. 3.3 and the self-energy in Subsec. 3.4 unambiguously demonstrate a decisive role of spin-fluctuations in renormalization

of the electronic spectrum in strongly correlated system as cuprate superconductors. With doping or temperature increasing, spin correlations are suppressed which results in transition from a strong to a weak coupling. This observation was confirmed by consideration of the intermediate Coulomb correlations in Subsec. 3.5.

Acknowledgments. One of the authors (N.P.) is grateful to Prof. P. Fulde for the hospitality extended to him during his stay at MPIPKS, Dresden, where a major part of the present work has been done.

REFERENCES

1. *Damascelli A., Hussain Z., Shen Z.-X.* // Rev. Mod. Phys. 2003. V. 75. P. 473.
2. *Eschrig M.* // Adv. Phys. 2006. V. 55. P. 47.
3. *Anderson P. W.* // Science. 1987. V. 235. P. 1196;
   Anderson P. W. The Theory of Superconductivity in the High-T_c Cuprates. Princeton: Princeton University Press, 1997.
4. *Bulut N.* // Adv. Phys. 2002. V. 51. P. 1587.
5. *Ovchinnikov G., Valkov V. V.* Hubbard Operators in the Theory of Strongly Correlated Electrons. London: Imperial College Press, 2004.
6. *Georges A., Kotliar G., Krauth W., Rozenberg M.* // Rev. Mod. Phys. 1996. V. 68. P. 13.
7. *Kotliar G., Savrasov S. Y., Haule K., Oudovenko V. S., Parcollet O., Marianetti C. A.* // Rev. Mod. Phys. (to be published); cond-mat/0511085.
8. *Maier Th., Jarrel M., Pruschke Th., Hettler M. H.* // Rev. Mod. Phys. 2005. V. 77. P. 1027.
9. *Tremblay A. M. S., Kyung B., Sénéchal D.* // Fizika Nizkikh Temperatur (J. Low Temp. Phys.). 2006. V. 32. P. 561.
10. *Sadovskii M. V., Nekrasov I. A., Kuchinskii E. Z., Pruschke Th., Anisimov V. I.* // Phys. Rev. B. 2005. V. 72. P. 155105.
11. *Zubarev D. N.* // Usp. Fiz. Nauk. 1960. V. 71. P. 71; Ibid. 1960. V. 3. P. 320.
12. *Mancini F., Avella A.* // Adv. Phys. 2004. V. 53. P. 537.
13. *Krivenko S., Avella A., Mancini F., Plakida N.* // Physica B. 2005. V. 359–361. P. 666.
14. *Kakehashi Y., Fulde P.* // Phys. Rev. B. 2004. V. 70. P. 195102; J. Phys. Soc. Jpn. 2005. V. 74. P. 2397.

15. *Plakida N. M., Hayn R., Richard J.-L.* // Phys. Rev. B. 1995. V. 51. P. 16599.

16. *Plakida N. M., Oudovenko V. S.* // Phys. Rev. B. 1999. V. 59. P. 11949.

17. *Plakida N. M., Anton L., Adam S., Adam Gh.* // Zh. Exp. Theor. Fiz. 2003. V. 124. P. 367; JETP. 2003. V. 97. P. 331.

18. *Feiner L. F., Jefferson J. H., Raimondi R.* // Phys. Rev. B. 1996. V. 53. P. 8751.

19. *Yushankhai V. Yu., Oudovenko V. S., Hayn R.* // Phys. Rev. B. 1997. V. 55. P. 15562.

20. *Emery V. J.* // Phys. Rev. Lett. 1987. V. 58. P. 2794;
Varma C. M., Schmitt-Rink S., Abrahams E. // Solid State Commun. 1987. V. 62. P. 681.

21. *Migdal A. B.* // Zh. Eksp. Teor. Fiz. 1956. V. 34. P. 1438; JETP. 1958. V. 7. P. 996.

22. *Eliashberg G. M.* // Zh. Eksp. Teor. Fiz. 1960. V. 38. P. 966; Ibid 1960. V. 39. P. 1437; JETP 1960. V. 11. P. 696; Ibid 1960. V. 12. P. 1000.

23. *Jaklič J., Prelovšek P.* // Phys. Rev. Lett. 1995. V. 74. P. 3411; Ibid. 1995. V. 75. P. 1340.

24. *Bonca J., Prelovšek P., Sega I.* // Europhys. Lett. 1989. V. 10. P. 87.

25. *Yoshida T. et al.* // Phys. Rev. B. 2001. V. 63. P. 220501.

26. *Kordyuk A. A., Borisenko S. V., Koitzsch A., Fink J., Knupfer M., Berger H.* // Phys. Rev. B. 2005. V. 71. P. 214513.

27. *Liu Z., Manousakis E.* // Phys. Rev. B. 1992. V. 45. P. 2425.

Received on July 4, 2006.